Volume 61
Number 54
11 July 2025
Pages 9723–9984

ChemComm

Chemical Communications

rsc.li/chemcomm

ISSN 1359-7345

ROYAL SOCIETY OF CHEMISTRY

COMMUNICATION

Tsuyoshi Minami *et al.*

Accurate determination of enantiomeric excess of an amino acid using an extended-gate-type organic transistor

ChemComm

COMMUNICATION

View Article Online
View Journal | View Issue

Cite this: *Chem. Commun.*, 2025, **61**, 9872

Received 19th April 2025,
Accepted 28th May 2025

DOI: 10.1039/d5cc02191j

rsc.li/chemcomm

Accurate determination of enantiomeric excess of an amino acid using an extended-gate-type organic transistor†

Yijing Zhang, [a] Yui Sasaki, [abc] Xiaojun Lyu, [a] Jun-ichi Ogawa,[d] Hidenosuke Itoh[d] and Tsuyoshi Minami *[a]

An extended-gate-type organic field effect transistor functionalized with molecularly imprinted polymer has shown chiral selectivity to L-histidine and discriminated it from amino acid families. Indeed, the chiral sensor device has simultaneously determined four points of the enantiomeric excesses of the chiral amino acid.

The homochirality of amino acids is a significant feature in biochemical processes.[1] In addition, chiral amino acids are essential components in various industrial fields, including pharmaceuticals, foods and drinks, cosmetics, *etc.*[2] Thus, the determination of enantiomeric excess (ee) of chiral amino acids is required in many fields. Enantiomeric purities of amino acids have been conventionally determined using high-performance liquid chromatography (HPLC) equipped with a chiral column.[3] Although the conventional method enables reliable chiral analysis, the requirements of large-sized apparatuses, trained personnel, and time-consuming measurements pose facile chiral detection. Thus, we propose a chemical sensor device for enantioselective detection and its ee determination with high accuracy. Among amino acids, L-histidine (His) was selected as the main target from the viewpoint of the detection significance in diagnosis.[4]

To date, various chiral receptors have been vigorously developed based on molecular recognition chemistry.[5] The fundamental strategy to design chiral receptors is the introduction of rigidity into a recognition scaffold, which is required for the discrimination of a slight structural difference in enantiomers.[5d,e] For example, rigid receptor skeletons such as atropisomers (*e.g.*, binaphthyl[5f] and benzophenone[5g]) and macrocycles (*e.g.*, cucurbit[*n*]uril[5h] and cyclodextrin[5i]) have been vigorously used for the discrimination of structural differences in amino acid families and their % ee determination. However, high synthetic efforts to obtain such rigid receptors that satisfy complementarity with chiral amino acids remain challenging tasks in sensing applications. In addition, the high rigidity of receptors causes low water solubility, which poses chiral sensing in aqueous media.[5f,g] To overcome the above issues, we here employed a molecular imprinting method to easily obtain chiral receptors without a synthetic burden and to perform chiral sensing in aqueous media.

Molecularly imprinted polymers (MIPs) are artificial recognition materials created by polymerization of functional monomers in the presence of templates (*i.e.*, analytes).[6] The specificity of MIPs is derived from three-dimensional recognition scaffolds provided by multiple interactions between functional monomers and templates. By selecting appropriate monomers, a MIP layer can be easily fabricated on an electrode through electrochemical polymerization.[6c,d] Therefore, a solid-state MIP layer on an electrode enables chiral sensing at an interface between the MIP electrode and aqueous media containing a chiral analyte.[6e] The chiral recognition information is visualized by connecting the electrode to an appropriate transducer unit.

A compact switching device based on a field-effect transistor (FET) has emerged as a promising platform for various applications.[7] The applicability of solution processes in device fabrication has accelerated the manufacturing of organic FET (OFET)-based chemical sensors.[8] By integrating appropriate molecular recognition materials, the OFET can demonstrate quantitative changes in transistor characteristics such as threshold voltages (V_{TH}s) and drain currents (I_{DS}s) upon analyte capture.[9] Notably, the amplification ability of OFETs contributes to sensitive detection over conventional electrochemical methods.[6d,e] Meanwhile, the instability of organic semiconductive layers of OFETs under

[a] *Institute of Industrial Science, The University of Tokyo, 4-6-1 Komaba, Meguro-ku, Tokyo, 153-8505, Japan. E-mail: tminami@g.ecc.u-tokyo.ac.jp*
[b] *Research Center for Advanced Science and Technology, The University of Tokyo, 4-6-1, Komaba, Meguro-ku, Tokyo, 153-8904, Japan*
[c] *JST PRESTO, 4-1-8 Honcho, Kawaguchi, Saitama, 332-0012, Japan*
[d] *Yokogawa Electric Corporation, 2-9-32 Nakacho, Musashino, Tokyo 180-0006, Japan*

† Electronic supplementary information (ESI) available: Regents and materials, apparatuses and methods, basic transistor characteristics, characterization of the MIP electrode, evaluation of the detectability of the MIP electrode, determination of enantiomeric purity of target histidine. See DOI: https://doi.org/10.1039/d5cc02191j

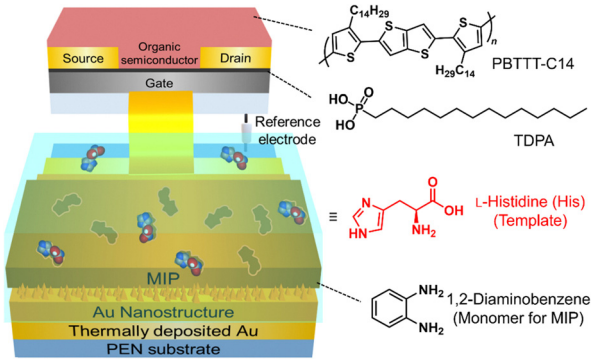

Fig. 1 Schematic illustration of an extended-gate-type OFET functionalized with MIP for chiral recognition and % ee determination of L-His and chemical structures of the sensor components. 1,2-Diaminobenzene was used as the functional monomer for MIP fabrication.

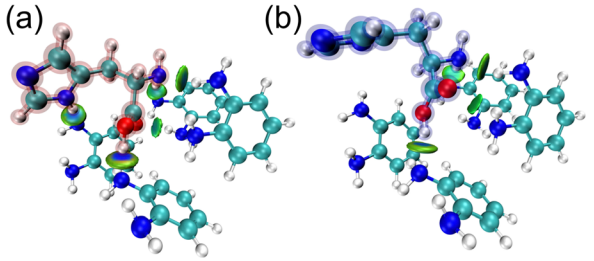

Fig. 2 The isosurface IGM figure of the optimized complexes of 1,2-diaminobenzene and (a) L- or (b) D-His at a 4 : 1 molar ratio. The blueish-green ellipsoid areas indicate non-covalent interactions.

ambient conditions is a bottleneck for chemical sensing in aqueous media.[10] Considering this, an extended-gate structure was selected as a configuration of a MIP-attached OFET-based chiral sensor (MIP-OFET) in this study.[11] The OFET device is isolated from a sensing gate in this structure, which qualitatively and quantitatively detects changes in transistor characteristics upon analyte capture at an electrode functionalized with a MIP layer for L-His (Fig. 1). To the best of our knowledge, the combination of organic transistors and MIPs have been applied to the detection of chiral amino acids, whereas the % ee determination has never been reported.[12] To this end, we strategically employed two crucial techniques using density functional theory (DFT) calculations for an optimal MIP design and a powerful machine learning method (*i.e.*, support vector machine, SVM) for accurate data analysis (*vide infra*).

In this study, 1,2-diaminobenzene was selected as a functional monomer for MIP against L-His (Fig. 1). The monomer can be polymerized on an Au electrode by an electrochemical method.[13] In addition, the polymerized structure is favorable for selective recognition based on multiple hydrogen bonds with a specific analyte.[6d] Herein, two hydrogen bonds between two monomers and one carboxy group of the template were expected. One of the monomers interacting with the carbonyl group could also contribute to a hydrogen bond with the primary amino group of L-His. The appropriate molar ratio between the monomer and the template was determined by both DFT calculations and experimental investigations. For example, the pre-organized structure at a 3 : 1 molar ratio (= 1,2-diaminobenzene: L-His) indicates insufficient interactions between the monomers and the template (Fig. S1(a), ESI†). Meanwhile, although a slightly more stable complex was observed at a 5 : 1 molar ratio, the surplus monomer did not contribute to interactions with the template (see the ESI†). In contrast, four monomers efficiently contributed to hydrogen bonds with all binding sites of the template at a 4 : 1 molar ratio (Fig. 2(a) and Fig. S2(a), ESI†). The isosurface figures of the Independent Gradient Model (IGM)[14] indicate pre-organized structures of 1,2-diaminobenzene and a template (*i.e.*, L- or D-His) at a 4 : 1 molar ratio (Fig. 2). The same conditions of fragments (*i.e.*, 1,2-diaminobenzene) that optimized for L-His were also applied to D-His in DFT calculations. The DFT calculations revealed a difference in the binding energy of the pre-organized structures between L-(-155.6 kJ mol^{-1}) and D-His (-122.3 kJ mol^{-1}) owing to the following reasons. The bluish-green ellipsoid areas suggest non-covalent interactions between the monomers and the chiral template (*i.e.*, L- or D-His). Among them, hydrogen bonds provided by the monomers contributed to interactions with the primary amino group and the carboxy group of L-His (Fig. 2(a) and Fig. S2(a), ESI†). The abovementioned interactions were also observed in the pre-organized structure of D-His, likewise L-His (Fig. 2(b) and Fig. S2(b), ESI†). On the other hand, a noncovalent interaction between the monomer and the secondary amino moiety of the imidazole ring of the template was only observed in the pre-organized structure with L-His, which implies a key interaction to distinguish L-His from D-His. According to the determined molar ratio, 1,2-diaminobenzene was electrochemically polymerized on an Au electrode in the presence of L-His. The surface of a thermally deposited Au electrode was modified by an Au nanostructure with a needle-like shape to enhance adhesion of the MIP layer to the extended-gate electrode.[6d,e] The conductivity of the Au extended-gate electrode decreased upon polymerization of 1,2-diaminobenzene by cyclic voltammetry (CV), which suggested the accumulation of an insulating polymer layer (Fig. S5, ESI†).[13] The extraction of the template from the polymerized electrode was performed by CV in a basic solution. The details of electrode fabrication are summarized in the ESI.†

Next, the detectability of the MIP electrode for L-His was evaluated by differential pulse voltammetry (DPV). The detection mechanism of the MIP made of 1,2-diaminobenzene for L-His relies on hydrogen bonds.[15] Thus, pH conditions for all chiral sensing were set to 6.0, considering the pK_a of His.[16] Fig. S6 (ESI†) displays a concentration-dependent decrease in currents of the MIP electrode upon adding L-His (0.0–10 mM) in a $K_3Fe(CN)_6$ solution. The phenomenon can be explained by the behavior of electroactive ions (*i.e.*, $[Fe(CN)_6]^{3-}$) inside the cavity of MIP on the Au electrode.[6c,17] In the absence of L-His, the electroactive ions inside the cavity of MIP can approach the Au electrode surface, whereas their approach was prevented by the capturing of L-His inside the cavity of MIP. Therefore, the current decrease upon adding L-His in the DPV measurement indicated the analyte capture by the MIP electrode.

Subsequently, the OFET was employed for chiral sensing. In the OFET fabrication, a combination of aluminum oxide and

tetradecylphosphonic acid was used as a dielectric layer to operate at low voltage ($<|3|$ V).[18] In addition, the semiconductive layer made of poly{2,5-bis(3-tetradecylthiophen-2-yl)thieno[3,2-*b*]thiophene}[19] was formed by a drop-casting process. The surface of the device was entirely covered with a hydrophobic material (*i.e.*, CYTOP™) for passivation. The basic transistor characteristics were evaluated under ambient conditions (Fig. S9, ESI†). The details of the device fabrication process and measurements are summarized in the ESI.† The manufactured OFET device and the MIP-attached extended-gate electrode were connected using a conductive cable to perform chiral sensing. The MIP-OFET showed concentration-dependent V_{TH} shifts upon adding L-His (0.0–1.0 mM) in a phosphate buffer solution (100 mM) at pH 6.0 at 25 °C (Fig. 3). Moreover, the limit of detection was estimated to be 73 μM based on the 3σ method.[20] In contrast to L-His, the MIP-OFET did not respond to D-His (Fig. 3). Although a slight fluctuation of the response to D-His due to the enantiomeric purity of commercially available L-His (94.9% ee determined by HPLC, Fig. S14, ESI†) used in MIP fabrication was observed, this demonstration revealed the high enantioselectivity of the MIP-OFET.

Furthermore, we investigated the discriminatory ability of the MIP-OFET to L-His from L-type aromatic amino acids (*i.e.*, tyrosine (Tyr), phenylalanine (Phe), and tryptophan (Trp)) and L-lysine (Lys). Fig. 4 displayed the highest response to L-His over other L-amino acids.[21] The selectivity test clarified the significance of the optimization of the MIP design considering interactions with the chiral template. Indeed, the DFT calculation results revealed the unstable complexation with L-type aromatic amino acids (*i.e.*, Tyr, Phe, or Trp) than L-His (Table S2, ESI†). As the next attempt, the MIP-OFET was applied to determine the % ee of L-His. In general, chemical sensors show non-linear responses in complicated sensing situations, which cause difficulty in the precise determination of analyte information. Thus, we decided to apply SVM for data processing of slight differences in transistor characteristics depending on the % ee changes (Fig. S15, ESI†). The SVM is one of the machine learning methods that is capable of building linear calibration lines even in non-linear responses.[22] In addition, the SVM enables the prediction of unknown chemical information based on the supervised dataset. In this assay, the transfer characteristics (V_{GS}–I_{DS}) of the MIP-OFET upon changing in % ee of L-His were collected to obtain an inset data for regression analysis using SVM (Fig. S15(a), ESI†). Fig. 5 shows the distribution of four predicted plots (*i.e.*, 13.9% ee, 23.4% ee, 51.9% ee, and 84.1% ee as orange square plots) on the calibration line (*i.e.*, gray circle plots). The values of the root-mean-square errors of calibration (RMSEC) and prediction (RMSEP) indicate the accuracy of the built model and predictions. The % ee determination against four test plots revealed the usability of the chiral sensor system combined with the SVM.

In summary, we demonstrated chiral analysis, especially % ee determination, using the extended-gate-type OFET functionalized with the MIP layer. The pre-organized structure of 1,2-diaminobenzene as the functional monomer and L-His as the template was optimized by using DFT calculations. In addition, the visualized structure clarified the significant noncovalent interaction of the monomer and the template to distinguish L-His from D-His. Indeed, the MIP-OFET showed chiral selective

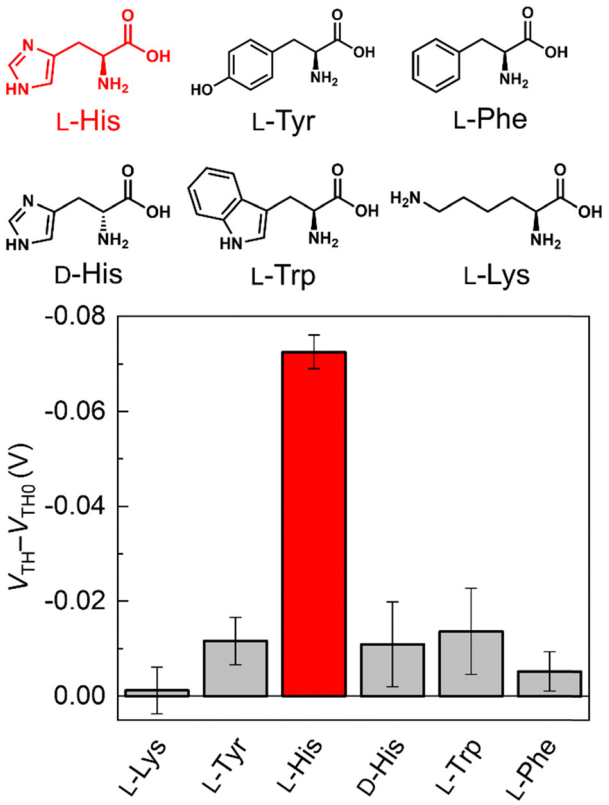

Fig. 4 Selectivity test results of the MIP-OFET for amino acids (1.0 mM) in a phosphate buffer solution (100 mM) at pH 6.0 at 25 °C. The terms V_{TH0} and V_{TH} mean threshold voltages before and after adding targets (n = 3).

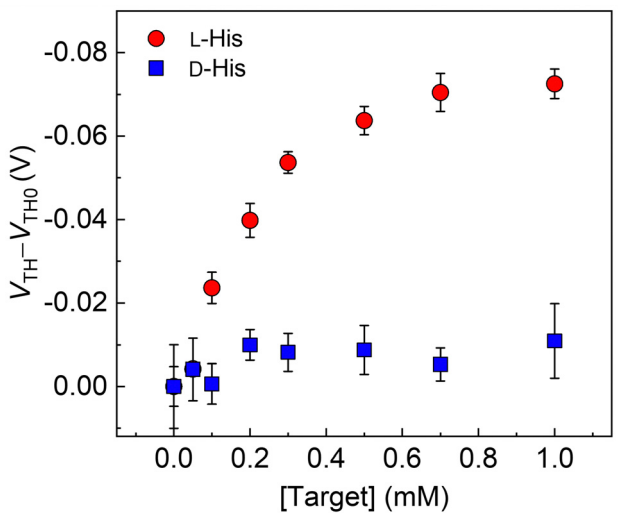

Fig. 3 Responses of the MIP-OFET to L-(red circles) and D-His (blue squares) in a phosphate buffer solution (100 mM) at pH 6.0 at 25 °C. The terms V_{TH0} and V_{TH} mean threshold voltages before and after adding targets (n = 3). The titration isotherms were obtained by collecting V_{TH}s at V_{GS} = −2 V.

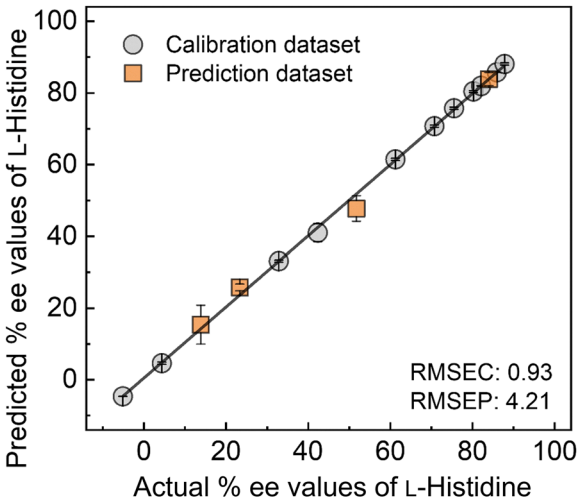

Fig. 5 Regression analysis using SVM for % ee determination of L-His.

response to L-His and discriminated from L-amino acid families. Finally, the % ee determination was conducted by applying SVM. The estimated % ee values based on the SVM analysis of the changes in the transistor characteristics indicated the feasibility of accurate chiral analysis without using a stationary apparatus. Through this demonstration, we revealed that the employment of calculation methods such as DFT and machine learning will not only expand the potential of conventional sensor technologies but also contribute to accurate analysis against challenging analytes.

Y. Sasaki gratefully acknowledges the financial support from the Japan Society for the Promotion of Science (JSPS) KAKENHI (Grant No. JP24K17667) and JST PRESTO (Grant No. JPMJPR23H2). T. Minami thanks JSPS KAKENHI (Grant No. JP23H03864 and JP24K01315) and JST CREST (Grant No. JPMJCR2011). All authors thank Miyuki Kato for performing HPLC analysis (Fig. S14, ESI†).

Conflicts of interest

There are no conflicts of interest to declare.

Data availability

The data supporting this article have been included as part of the ESI.†

Notes and references

1 A. Banreti, S. Bhattacharya, F. Wien, K. Matsuo, M. Réfrégiers, C. Meinert, U. Meierhenrich, B. Hudry, D. Thompson and S. Noselli, *Nat. Commun.*, 2022, **13**, 7059.
2 Y.-P. Xue, C.-H. Cao and Y.-G. Zheng, *Chem. Soc. Rev.*, 2018, **47**, 1516–1561.
3 (*a*) I. Ilisz, R. Berkecz and A. Péter, *J. Sep. Sci.*, 2006, **29**, 1305–1321; (*b*) G. Carenzi, S. Sacchi, M. Abbondi and L. Pollegioni, *Amino Acids*, 2020, **52**, 849–862.
4 (*a*) J. Y. Oh, Y. S. Lee, K. H. Min, G. Y. Hur, S. Y. Lee, K. H. Kang, C. K. Rhee, S. J. Park, A. Khan, J. Na, Y. H. Park and J. J. Shim, *Int. J. Chronic Obstruct. Pulm. Dis.*, 2018, **13**, 1809–1818; (*b*) Y. Okusha, Y. Hirai, H. Maezawa, K. Hisadome, N. Inoue, Y. Yamazaki and M. Funahashi, *J. Physiol. Sci.*, 2017, **67**, 467–474.
5 For reviews, see: (*a*) M. Hu, H.-T. Feng, Y.-X. Yuan, Y.-S. Zheng and B. Z. Tang, *Coord. Chem. Rev.*, 2020, **416**, 213329; (*b*) M. Quan, X.-Y. Pang and W. Jiang, *Angew. Chem., Int. Ed.*, 2022, **61**, e202201258; (*c*) J. Guo, J. Hou, J. Hu, Y. Geng, M. Li, H. Wang, J. Wang and Q. Luo, *Chem. Commun.*, 2023, **59**, 9157–9166; (*d*) J. S. S. K. Formen, J. R. Howard, E. V. Anslyn and C. Wolf, *Angew. Chem., Int. Ed.*, 2024, **63**, e202400767. For examples, see: (*e*) Y. Sasaki, S. Kojima, V. Hamedpour, R. Kubota, S. Takizawa, I. Yoshikawa, H. Houjou, Y. Kubo and T. Minami, *Chem. Sci.*, 2020, **11**, 3790–3796; (*f*) Y.-Y. Zhu, X.-D. Wu, S.-X. Gu and L. Pu, *J. Am. Chem. Soc.*, 2019, **141**, 175–181; (*g*) H. Kim, S. M. So, C. P.-H. Yen, E. Vinhato, A. J. Lough, J.-I. Hong, H.-J. Kim and J. Chin, *Angew. Chem., Int. Ed.*, 2008, **47**, 8657–8660; (*h*) T. Minami, N. A. Esipenko, B. Zhang, L. Isaacs and P. Anzenbacher, Jr., *Chem. Commun.*, 2014, **50**, 61–63; (*i*) Y. Sun, Y. Wang, Y. Wu, X. Wang, X. Li, S. Wang and Y. Xiao, *Anal. Chem.*, 2018, **90**, 9264–9271.
6 For reviews, see: (*a*) K. Haupt, P. X. Medina Rangel and B. T. S. Bui, *Chem. Rev.*, 2020, **120**, 9554–9582; (*b*) T. Takeuchi and H. Sunayama, *Chem. Commun.*, 2018, **54**, 6243–6251For examples, see: (*c*) Q. Zhou, M. Wang, S. Yagi and T. Minami, *Nanoscale*, 2021, **13**, 100–107; (*d*) Y. Sasaki, Y. Zhang, H. Fan, K. Ohshiro, Q. Zhou, W. Tang, X. Lyu and T. Minami, *Sens. Actuators, B*, 2023, **382**, 133458; (*e*) Q. Zhou, Y. Sasaki, K. Ohshiro, H. Fan, V. Montagna, C. Gonzato, K. Haupt and T. Minami, *J. Mater. Chem. B*, 2022, **10**, 6808–6815.
7 G. Horowitz, *Adv. Mater.*, 1998, **10**, 365–377.
8 T. Minamiki, T. Minami, Y.-P. Chen, T. Mano, Y. Takeda, K. Fukuda and S. Tokito, *Commun. Mater.*, 2021, **2**, 8.
9 Y. Sasaki and T. Minami, *Phys. Status Solidi A*, 2023, **220**, 2300469.
10 M. E. Roberts, S. C. B. Mannsfeld, N. Queraltó, C. Reese, J. Locklin, W. Knoll and Z. Bao, *Proc. Natl. Acad. Sci. U. S. A.*, 2008, **105**, 12134–12139.
11 (*a*) J. van der spiegel, I. Lauks, P. Chan and D. Babic, *Sens. Actuators*, 1983, **4**, 291–298; (*b*) Y. Sasaki, K. Ohshiro, X. Lyu, T. Kawashima, M. Kamiko, H. Tanaka, A. Yamagami, Y. Ueno and T. Minami, *Chem. Commun.*, 2024, **60**, 9930–9933.
12 (*a*) L. Zhang, Z. Liu, C. Xiong, L. Zheng, Y. Ding, H. Lu, G. Zhang and L. Qiu, *Org. Electron.*, 2018, **61**, 254–260; (*b*) Z. Iskierko, A. Checinska, P. S. Sharma, K. Golebiewska, K. Noworyta, P. Borowicz, K. Fronc, V. Bandi, F. D'Souza and W. Kutner, *J. Mater. Chem. C*, 2017, **5**, 969–977.
13 S. Bilal, A.-U.-H. A. Shah and R. Holze, *Electrochim. Acta*, 2012, **85**, 358–368.
14 C. Lefebvre, G. Rubez, H. Khartabil, J.-C. Boisson, J. Contreras-García and E. Hénon, *Phys. Chem. Chem. Phys.*, 2017, **19**, 17928–17936.
15 R. N. V. Krishna Deepak and R. Sankararamakrishnan, *Biochemistry*, 2016, **55**, 3774–3783.
16 M. Hennig and B. H. Geierstanger, *J. Am. Chem. Soc.*, 1999, **121**, 5123–5126.
17 S. Motia, B. Bouchikhi, E. Llobet and N. El Bari, *Talanta*, 2020, 216, 120953.
18 H. Klauk, U. Zschieschang, J. Pflaum and M. Halik, *Nature*, 2007, **445**, 745–748.
19 I. McCulloch, M. Heeney, C. Bailey, K. Genevicius, I. MacDonald, M. Shkunov, D. Sparrowe, S. Tierney, R. Wagner, W. Zhang, M. L. Chabinyc, R. J. Kline, M. D. McGehee and M. F. Toney, *Nat. Mater.*, 2006, **5**, 328–333.
20 J. N. Miller and J. C. Miller, *Statistics and Chemometrics for Analytical Chemistry*, Pearson Education Canada, 5th edn, 2005.
21 Weak responses to other amino acids were observed in the selectivity test. In this regard, a polymerized layer without using the template exhibited a weak DPV current response toward L-His (Fig. S7, ESI†). Thus, the observed responses to other amino acids were presumably derived from physical adsorption to the MIP electrode.
22 (*a*) T. Minami, N. A. Esipenko, B. Zhang, M. E. Kozelkova, L. Isaacs, R. Nishiyabu, Y. Kubo and P. Anzenbacher Jr., *J. Am. Chem. Soc.*, 2012, **134**, 20021–20024; (*b*) L. Hamel, *Knowledge Discovery with Support Vector Machines*, John Wiley & Sons, Inc., 2009.